PHARMACOKINETIC MODELS IN CLINICAL PRACTICE: WHAT MODEL TO USE FOR DCE-MRI OF THE BREAST?

G.J.S. Litjens[1], *M. Heisen*[1], *J. Buurman*[2], *B.M. ter Haar Romeny*[1]

[1]Eindhoven University of Technology, Department of Biomedical Engineering
5612AV Eindhoven, The Netherlands
[2]Philips Healthcare, Healthcare Informatics
5684 PC Best, The Netherlands

ABSTRACT

Pharmacokinetic modeling is increasingly used in DCE-MRI high risk breast cancer screening. Several models are available. The most common models are the standard and extended Tofts, the shutter-speed, and the Brix model. Each model and the meaning of its parameters is explained. It was investigated which models can be used in a clinical setting by simulating a range of sampling rates and noise levels representing different MRI acquisition schemes. In addition, an investigation was performed on the errors introduced in the estimates of the pharmacokinetic parameters when using a physiologically less complex model, i.e. the standard Tofts model, to fit curves generated with more complex models. It was found that the standard Tofts model is the only model that performs within an error margin of 20% on parameter estimates over a range of sampling rates and noise levels. This still holds when small complex physiological effects are present.

Index Terms— Pharmacokinetic modeling, breast cancer, sampling time, DCE-MRI

1. INTRODUCTION

Dynamic contrast-enhanced magnetic resonance imaging (DCE-MRI) has shown to be a valuable tool in diagnosis of breast cancer [1]. A Gd-DTPA based contrast agent (CA) is injected and T_1-weighted scans are made over time. In addition to assessment of morphological features the kinetic behavior of the CA uptake has diagnostic potential [2]. However, descriptive features like signal enhancement ratio (as a measure of washout) seem to have limited value due to variations in patient physiology and injection protocol [3]. To remove these dependencies and obtain tumor-specific parameters, pharmacokinetic models were developed [4]. Over the past decade several models have become available for the analysis of the concentration-time curves of DCE-MRI. These models describe the diffusion of the CA from the blood pool into the extracellular space; each using different assumptions and simplifications. In this paper it is investigated if and which of these models can be used reliably for clinical data. The most prominent problem in clinical data acquisition when using these models is the sampling time (often 1-2 min) with which images are acquired. This sampling time is important because of the Nyquist-Shannon sampling criterion. In image acquisition a balance has to be found between image quality (SNR, spatial resolution) and sampling time, thus it was investigated if the use of certain models is restrained by this tradeoff.

2. MATERIALS AND METHODS

Common pharmacokinetic models are the standard and extended Tofts models [5] (most used in literature); the shutter-speed model [6] (incorporates water-exchange effects); and the Brix model [7] (separate estimates of flow and permeability). This Brix model is based on the exchange model by Morales and Smith [8], as opposed to the other three models which are based on the exchange model by Kety [8].

The Tofts models consist of two and three parameters respectively. In the standard Tofts model [Eq. 1] K^{trans} is a combined measure of blood flow and capillary permeability (min^{-1}), whereas it only presents permeability in the extended model [Eq. 2] (under the assumption of fast blood flow). In both models, v_e is the volume fraction of extracellular, extravascular space (EES) within a voxel. The additional parameter used in the extended Tofts model is v_p , the fraction of blood plasma within a voxel.

$$C_t[t] = K^{\text{trans}} \int_0^t e^{-\frac{K^{\text{trans}}}{v_e}(t-s)} C_p[s]ds \tag{1}$$

$$C_t[t] = K^{\text{trans}} \int_0^t e^{-\frac{K^{\text{trans}}}{v_e}(t-s)} C_p[s]ds + v_p C_p[t] \tag{2}$$

$C_p[t]$ is the concentration (mM) of CA in the blood plasma and $C_t[t]$ the concentration (mM) in the tissue of interest. Time t (min) is the time that has passed since CA injection.

The shutter-speed model [Eq. 3] is different in that it also incorporates the effect of water exchange on the MRI signal amplitude. Because the CA cannot enter the intracellular space (IS) it only has a direct effect on the water protons in the EES. The other models assume that the water exchange between those spaces is infinitely fast, essentially stating that the contrast agent can influence all water. The shutter-speed model does not use this assumption. For a thorough derivation the reader is referred to [6]. This model introduces the extra parameter τ_i (s) which is the mean time that a water proton is in the IS. In essence this model is not a pharmacokinetic model, as it uses the standard Tofts model to represent the pharmacokinetic part of the equation. The shutter-speed part models the MRI effects and thus gives R_1[t] (s^{-1}), the longitudinal relaxation rate. Time in this model is usually expressed in seconds.

$$R_1[t] = \frac{1}{2}\left(C_t[t]r_1 + R_{1_i}[0] + A_1 + \frac{1}{\tau_i} + A_2\right) - \frac{1}{2}\sqrt{\left(-C_t[t]r_1 + R_{1_i}[0] - A_1 + \frac{1}{\tau_i} - A_2\right)^2 + A_3} \tag{3}$$

$$A_1 = \frac{R_1[0] - (1-p_e)\,R_{1_i}[0]}{p_e}, \quad A_2 = \frac{1-p_e}{p_e \tau_i}$$
$$A_3 = \frac{4\,(1-p_e)}{p_e \tau_i^2}$$

Here, r_1 is the relaxivity of the contrast agent, which is approximately 3.8 $(\text{mM}^{-1})s^{-1}$ [6]. $R_1[0]$ (s^{-1}) and $R_{1_i}[0]$ (s^{-1}) are the relaxation rates in the absence of CA for the entire tissue and the IS respectively. They are kept constant at .67 and .69 s^{-1} [6]. p_e is the fractional water population of the EES ($p_e = .8 \cdot v_e$). [6].

The Brix model [Eq. 4] has an independent measure for relative blood flow $\frac{F}{r}$ (min^{-1}) in addition to K^{trans} (min^{-1}), which represents only permeability in this model, v_e and v_p .

$$\begin{aligned} v_p \frac{dC_c[t]}{dt} &= \frac{F}{r}\left(C_p[t] - C_c[t]\right) - K^{\text{trans}}\left(C_c[t] - C_e[t]\right) \\ v_e \frac{dC_e[t]}{dt} &= K^{\text{trans}}\left(C_c[t] - C_e[t]\right) \\ C_t &= v_p C_p + v_e C_e \end{aligned} \tag{4}$$

Here r a constant fraction between arterial, venous and tissue concentration. For the complete derivation the reader is referred to [7].

To investigate the differences in the errors of parameter estimation in clinical data, independent of the actual parameter values, forward-backward simulations were performed. The arterial input function (AIF) by Parker et al. [9] was used. Using latin hypercube sampling [10], a set of parameters was selected from a predefined range and a concentration-time curve was calculated using one of the four models. Values ranging from 0 to 1.5 min^{-1} were used for K^{trans} and for v_e values ranging from .1 to .6 [11]. For v_p a range of $0 < v_p \leq 0.2$[12] was found. For τ_i a range of 0 to 1.5 s was used [6] and for F a range of 1 to 6 min^{-1} [7].

The concentration-time curve was undersampled and Gaussian noise was added to represent concentration uncertainty due to for example noise in the images. For the range of sampling rates and noise levels clinical data from the University of Chicago Medical Center was used. 23 Datasets with a high sampling rate during the initial slope of the concentration-time curve were obtained in addition to the regular clinical scans that have a low sampling rate (due to high image quality constraints). The advantage of this protocol is that morphology can be assessed using the high quality (high SNR, high spatial resolution) images, and kinetics using the complete series. A low sampling rate after peak enhancement has been reached ($\sim$ 90 seconds) does not violate the Nyquist-Shannon criterion because the latter part does not contain high frequencies. In our simulation study the range of sampling rates is from 10 images to 50 images in the first 90 seconds [11]. The added noise level is in multiples of $1/3$ (varying between 0 and 2) times the level of uncertainty calculated from the clinical data. This level is around 8% of the concentration maximum in a curve, which is similar to values reported in literature [13]. This uncertainty is not only based on image noise but also on uncertainties in T_1-estimation, which is needed to convert signal intensity to concentration.

The selected model is fitted to this curve using the downhill Simplex method [14], with equalized weights for the initial and latter part of the curve. The resulting parameter estimates can be compared to the ones used to generate the concentration-time curve. The percentage of error was defined as:

$$\text{Error} = 100\left|\frac{P_i^{\text{Ori}} - P_i^{\text{Fit}}}{P_i^{\text{Ori}}}\right| \tag{5}$$

Here P_i is the i^{th} pharmacokinetic parameter.

For every combination (sampling rate + uncertainty level) and every model 500 simulations were performed using different pharmacokinetic parameter values. The errors were calculated and the means and standard deviations determined for every sampling rate-uncertainty combination.

In addition, it was also investigated what the effect of using the standard Tofts model is when the underlying assumptions are not true. This model was chosen because it uses the most assumptions. This was tested with a sampling rate of 20 images in the first 90 seconds and an added noise level equal of 8% of the concentration maximum. Concentration-time curves were simulated using either the Brix or shutter-speed models with different values for F , v_p and τ_i . These curves were fitted with the standard Tofts model and the error in K^{trans} and v_e was determined. For the standard Tofts/Brix combination 3000 simulations and for the standard Tofts/shutter-speed combination 1000 simulations were performed.

3. RESULTS

The mean and standard deviation of the errors at each combination of sampling rate and noise level were used to create a table with confidence intervals for every parameter of each model. It was found that the error distribution was not a normal distribution (Jarque-Bera test [15]), therefore the central limit theorem cannot be used. Chebyshev's inequality [16] could still be used however, which is a worst case measure for any distribution. A 90% confidence interval was constructed by using the one-sided variant of this rule, which states that the mean $\pm$ 3 standard deviations forms a 90% confidence interval.

A boundary has to be defined for the error measure at which the use of the model is rejected. In literature, values for benign and malignant tissue have been measured using the standard Tofts model and there seems to be separation between classes [11, 17]. Parameter values between those classes differ up from 20% on average, although large standard deviations still cause problems in cluster separation. Here, any parameter estimation with an error confidence interval higher than 20% was rejected.

In table 1a the results of the standard Tofts model are shown and it can be seen that confidence intervals for parameters are acceptable except for 10 images in 90 seconds. The extended Tofts model (table 1c) performs well on K^{trans} and v_e for 40 and 50 images per 90 seconds, however the estimates of v_p are not reliable. As this estimate is essentially the added value of this model its use is questionable for these types of data. The shutter-speed model (table 1d) has the same issue as the extended Tofts model in that is has good estimates of K^{trans} and v_e , but the errors on the added extra parameter τ_i are higher than 20%, so there is no added value compared to the standard Tofts model. The Brix model (table 1b) showed no changes over differences in added noise level so the results shown here are only for differences in sampling rate. What can be seen is that the model performance is bad over all sampling rates and does not reach acceptable error levels. For all models the sampling rate is of greater importance in reducing errors than the added noise level, except when sampling rates are already high (30 images per 90 seconds and more).

In addition to incorporating more parameters that could be of diagnostic value, the more complex models also reduce the number of assumptions. As the standard Tofts model has the most assumptions it is illustrative to look into the effects on the error measure if these assumptions are wrong. In figure 1ab the mean error in the estimates of K^{trans} and v_e are shown for simulations of concentration-time curves with the Brix model and fitting with the standard Tofts

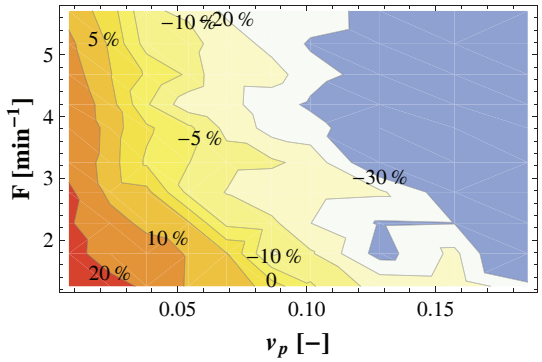

(a) Average error on K^{trans} when Brix model effects are present ($v_p > 0$, $F \downarrow 0$). Values of extra parameters in the Brix model are shown on the axes and the corresponding mean error value is shown on the contour line

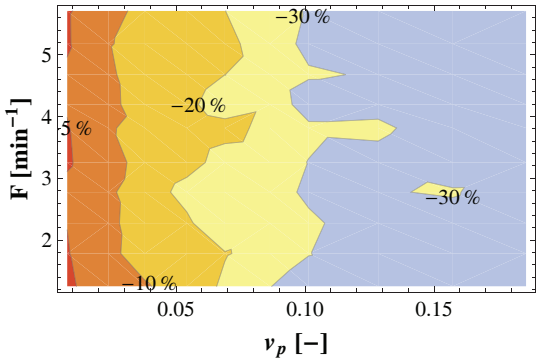

(b) Average error on v_e when Brix model effects are present ($v_p > 0$, $F \downarrow 0$). Values of extra parameters in the Brix model are shown on the axes and the corresponding mean error value is shown on the contour line

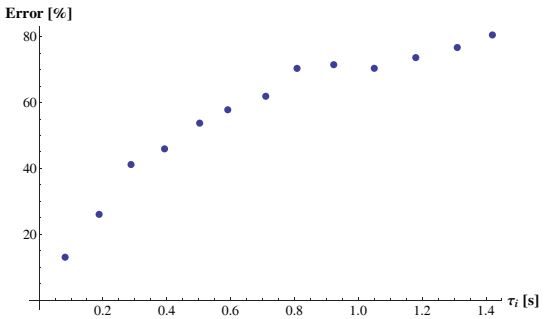

(c) Average error on K^{trans} when shutter-speed model effects are present ($\tau_i > 0$). Value of τ_i in the shutter-speed model is shown on the x-axis.

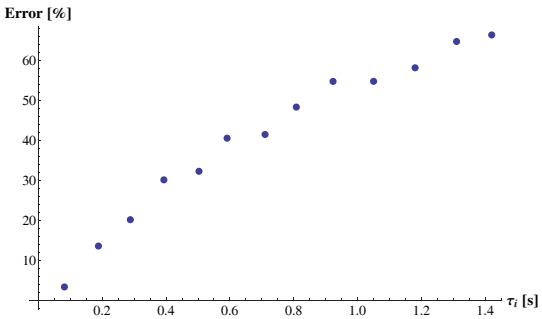

(d) Average error on v_e when shutter-speed model effects are present ($\tau_i > 0$). Value of τ_i in the shutter-speed model is shown on the x-axis.

Fig. 1. Errors of using a physiologically simple model to model a physiologically complex process

model. It can be seen that the value of F has little influence on the estimation of K^{trans} and v_e , the contour line density is low perpendicular to the y-axis. For v_p the results are different, for substantial increases in v_p the errors in parameter estimates can increase significantly, which can be seen because the contour lines density is higher.

In figure 1c and d the results for simulating concentration-time curves with the shutter-speed model and fitting with the standard Tofts are shown. From these figures it can be concluded that it is very important to know the values of τ_i to expect in breast cancer, its exclusion can have a large influence on the increase in average error.

4. DISCUSSION

It can be concluded that the errors in the standard Tofts model parameters are low enough to be used in clinical data when the assumptions underlying this model approximately hold. For the other models the use in clinical settings is doubtful because demands on the sampling time are much higher than those on the standard Tofts model, causing errors to be large for clinical values of sampling time and noise level. In addition it can be seen that when underlying assumptions are false, deviations from these assumptions can cause significant errors. Of these assumptions the infinitely fast water exchange is the most sensitive one, so more research should be focussed towards assessing the role of this effect in DCE-MRI for breast cancer.

The simulations were performed with the AIF known. However, in practice, this is not the case. At the moment most research uses AIFs from either literature or estimated from a large artery. Reference tissue methods for AIF determination are quickly gaining popularity and enable quite accurate reconstruction of the AIF from the image data itself [18]. In future research the effects of AIF determination on the errors in parameter estimation should be assessed. It can be concluded that it is possible to acquire high temporal resolution images in the initial part of the curve in addition to high quality images in the latter part of the curve for morphological assessment and still fit a pharmacokinetic model successfully. This means that radiologists do not necessarily have to choose between one or the other. As scan time is precious, this is an important advantage.

5. REFERENCES

[1] C. Kuhl, "The current status of Breast MR Imaging," *Radiology*, vol. 244, pp. 356–378, 2007.

[2] C. Kuhl and P. Mielcareck et al., "Dynamic breast mr imaging," *Radiology*, vol. 211, pp. 101–110, 1999.

[3] H. Aerts and N. van Riel et al., "System Identification Theory in Pharmacokinetic Modeling of Dynamic Contrast-Enhanced MRI," *Magnetic Resonance in Medicine*, vol. 59, pp. 1111–1119, 2008.

[4] P. Tofts and B. Berkowitz et al., "Quantitative analysis of Dynamic Gd-DTPA Enhancement in Breast Tumors using a Permeability Model," *Magnetic Resonance in Medicine*, vol. 33, pp. 564–568, 1995.

(a) Standard Tofts Model: K^{trans} and v_e

		K^{trans}							v_e						
		Noise level multiplier							**Noise level multiplier**						
		$\frac{0}{3}$	$\frac{1}{3}$	$\frac{2}{3}$	$\frac{3}{3}$	$\frac{4}{3}$	$\frac{5}{3}$	$\frac{6}{3}$	$\frac{0}{3}$	$\frac{1}{3}$	$\frac{2}{3}$	$\frac{3}{3}$	$\frac{4}{3}$	$\frac{5}{3}$	$\frac{6}{3}$
Nr. images	**10**	23	23	25	25	26	32	32	7	7	7	7	8	8	7
	20	9	12	15	16	17	19	20	6	7	7	7	8	7	8
	30	7	9	11	14	15	16	16	6	6	7	7	7	7	7
	40	7	8	10	11	13	13	14	6	6	6	7	6	7	7
	50	6	7	9	10	12	12	14	6	6	6	7	7	7	7

(b) Brix Model: F , K^{trans} , v_e , v_p

		Parameters			
		F	K^{trans}	v_e	v_p
Nr. images	**10**	119	56	35	154
	20	95	20	22	78
	30	93	20	26	83
	40	82	17	18	62
	50	76	19	19	53

(c) Extended Tofts Model: K^{trans} , v_e and v_p

		K^{trans}							v_e							v_p						
		Noise level multiplier							**Noise level multiplier**							**Noise level multiplier**						
		$\frac{0}{3}$	$\frac{1}{3}$	$\frac{2}{3}$	$\frac{3}{3}$	$\frac{4}{3}$	$\frac{5}{3}$	$\frac{6}{3}$	$\frac{0}{3}$	$\frac{1}{3}$	$\frac{2}{3}$	$\frac{3}{3}$	$\frac{4}{3}$	$\frac{5}{3}$	$\frac{6}{3}$	$\frac{0}{3}$	$\frac{1}{3}$	$\frac{2}{3}$	$\frac{3}{3}$	$\frac{4}{3}$	$\frac{5}{3}$	$\frac{6}{3}$
Nr. images	**10**	56	67	70	74	70	66	64	56	59	58	60	57	61	56	126	122	123	122	123	128	129
	20	28	34	39	41	41	39	47	30	34	35	33	35	34	37	85	83	87	79	83	93	87
	30	21	24	25	27	26	30	29	21	21	22	24	23	25	25	57	59	58	59	63	61	60
	40	13	16	18	18	23	31	27	16	17	18	16	20	28	20	41	41	44	44	43	74	47
	50	13	16	15	16	17	19	23	13	15	15	16	16	17	18	35	34	36	33	34	36	37

(d) Shutter Speed Model: K^{trans} , v_e and τ_i

		K^{trans}							v_e							τ_i						
		Noise level multiplier							**Noise level multiplier**							**Noise level multiplier**						
		$\frac{0}{3}$	$\frac{1}{3}$	$\frac{2}{3}$	$\frac{3}{3}$	$\frac{4}{3}$	$\frac{5}{3}$	$\frac{6}{3}$	$\frac{0}{3}$	$\frac{1}{3}$	$\frac{2}{3}$	$\frac{3}{3}$	$\frac{4}{3}$	$\frac{5}{3}$	$\frac{6}{3}$	$\frac{0}{3}$	$\frac{1}{3}$	$\frac{2}{3}$	$\frac{3}{3}$	$\frac{4}{3}$	$\frac{5}{3}$	$\frac{6}{3}$
Nr. images	**10**	75	74	75	79	78	85	78	44	44	43	45	47	50	41	62	71	73	62	70	77	68
	20	50	54	56	56	60	61	61	29	30	31	31	31	30	33	41	39	44	45	54	43	47
	30	41	44	48	49	50	48	50	23	23	26	25	24	24	25	30	31	36	35	32	44	42
	40	37	41	38	40	41	41	40	19	21	21	21	20	22	21	24	26	30	28	30	30	30
	50	34	35	34	38	34	35	36	17	17	18	20	18	17	19	26	24	29	26	31	26	29

Table 1. Error values in percentages on parameter estimates for a 90% confidence interval when using different numbers of images in first 90 seconds of enhancement (y-axis) and added noise levels (x-axis). The values in the table can be explained as that for a parameter it can be stated that for 90 of 100 cases its estimation will have an error between 0% and the value given

[5] P. Tofts, "Modeling tracer kinetics in dynamic Gd-DTPA MR imaging," *Journal of Magnetic Resonance Imaging*, vol. 7, pp. 91–101, 1997.

[6] T. Yankeelov and C. Springer et al., "Variation of the Relaxographic Shutter-Speed for Transcytolemmal Water Exchange Affects the CR Bolus-Tracking Curve Shape," *Magnetic Resonance in Medicine*, vol. 50, pp. 1151–1169, 2003.

[7] G. Brix and F. Kiessling et al., "Microcirculation and Microvasculature in Breast Tumors," *Magnetic Resonance in Medicine*, vol. 52, pp. 420–429, 2004.

[8] S. Kety, "The theory and applications of the exchange of inert gas at the lungs and in tissue," *Pharmacological review*, vol. 3, pp. 1–41, 1951.

[9] G. Parker and C. Roberts et al., "Experimentally-Derived Functional Form for a Population-Averaged High-Temporal-Resolution AIF," *Magnetic Resonance in Medicine*, vol. 56, pp. 993–1000, 2006.

[10] R.L. Iman and J.C. Helton et al., "An approach to sensitivity analysis of computer models.," *Journal of Quality Technology*, vol. 13, 1981.

[11] P. Eliat and V. Dedieu, "Magnetic resonance imaging contrast-enhanced relaxometry of breast tumors," *Magnetic Resonance Imaging*, vol. 22, pp. 475–481, 2004.

[12] H. Daldrup and D. Shames et al., "Quantification of the extraction fraction for gadopentetate across breast cancer capillaries," *Magnetic Resonance in Medicine*, vol. 40, pp. 537–543, 2005.

[13] R. Lopata and W. Backes et al., "On the Identifiability of Pharmacokinetic Parameters in Dynamic Contrast-Enhanced Imaging," *Magnetic Resonance in Medicine*, vol. 51, pp. 425–429, 2007.

[14] J. Nelder and R. Mead, "A simplex method for function minimization," *Computer Journal*, vol. 7, 1965.

[15] C. Jarque and A. Bera, "Efficient tests for normality, homoscedasticity and serial independence of regression residuals," *Economic Letters*, vol. 6, pp. 255–259, 1980.

[16] A. Papoulis, *Probability, Random Variables, and Stochastic Processes*, McGraw-Hill, 1991.

[17] C. Hulka and B.Smith et al., "Benign and malignant breast lesions: Differentiation with echo-planar MR imaging," *Radiology*, vol. 197, pp. 33–38, 1995.

[18] T. Yankeelov and J. Luci et al., "Quantitative pharmacokinetic analysis of DCE-MRI data without an arterial input function: a reference region model," *Magnetic Resonance Imaging*, vol. 23, pp. 519–529, 2005.